Abnormal Cone and Rod Photoreceptor Morphogenesis in *gdf6a* Mutant Zebrafish

Nathan J. Nadolski,[1] Spencer D. Balay,[2,3] Casey X. L. Wong,[2,4] Andrew J. Waskiewicz,[4,5,6] and Jennifer C. Hocking[1–3,6]

[1]Department of Medical Genetics, University of Alberta, Edmonton, Alberta, Canada
[2]Division of Anatomy, Department of Surgery, University of Alberta, Edmonton, Alberta, Canada
[3]Department of Cell Biology, University of Alberta, Edmonton, Alberta, Canada
[4]Department of Biological Sciences, University of Alberta, Edmonton, Alberta, Canada
[5]Neuroscience and Mental Health Institute, University of Alberta, Edmonton, Alberta, Canada
[6]Women & Children's Health Research Institute, University of Alberta, Edmonton, Alberta, Canada

Correspondence: Jennifer C. Hocking, University of Alberta, 5-01 Medical Sciences Building, Edmonton, Alberta T6G 2H7, Canada; jhocking@ualberta.ca.

PURPOSE. Analysis of photoreceptor morphology and gene expression in mispatterned eyes of zebrafish *growth differentiation factor 6a* (*gdf6a*) mutants.

METHODS. Rod and cone photoreceptors were compared between *gdf6a* mutant and control zebrafish from larval to late adult stages using transgenic labels, immunofluorescence, and confocal microscopy, as well as by transmission electron microscopy. To compare transcriptomes between larval *gdf6a* mutant and control zebrafish, RNA-Seq was performed on isolated eyes.

RESULTS. Although rod and cone photoreceptors differentiate in *gdf6a* mutant zebrafish, the cells display aberrant growth and morphology. The cone outer segments, the light-detecting sensory endings, are reduced in size in the mutant larvae and fail to recover to control size at subsequent stages. In contrast, rods form temporarily expanded outer segments. The inner segments, which generate the required energy and proteins for the outer segments, are shortened in both rods and cones at all stages. RNA-Seq analysis provides a set of misregulated genes associated with the observed abnormal photoreceptor morphogenesis.

CONCLUSIONS. *GDF6* mutations were previously identified in patients with Leber congenital amaurosis. Here, we reveal a unique photoreceptor phenotype in the *gdf6a* mutant zebrafish whereby rods and cones undergo abnormal maturation distinct for each cell type. Further, subsequent development shows partial recovery of cell morphology and maintenance of the photoreceptor layer. By conducting a transcriptomic analysis of the *gdf6a* larval eyes, we identified a collection of genes that are candidate regulators of photoreceptor size and morphology.

Keywords: cone photoreceptor, rod photoreceptor, retinal pigmented epithelium, RNA-Seq, gdf6a

Photoreceptors are specialized light-detecting cells of the retina, and frequently the first cells lost in retinal dystrophies.[1] The sensory ending of each photoreceptor is a modified and expanded cilium, called the outer segment, which is packed with stacked membranous disks laden with photopigment.[2,3] Because the outer segment is densely occupied with the phototransduction machinery, the adjacent inner segment produces the protein and energy required for outer segment functioning and renewal.[4] The inner and outer segments are joined by the narrow connecting cilium, a region equivalent to the transition zone of primary cilia and through which proteins are constantly shuttled.[5]

Cone photoreceptors, which dominate the human central retina, mediate color and high-acuity vision, while the more peripheral and very sensitive rod photoreceptors mediate low light vision.[6] Beyond their differential responses to particular wavelengths and intensity of light, rods and cones also diverge in terms of cellular morphology.[2,3] Rod outer segments have a cylindrical shape and the membranous disks are enclosed within an outer layer of plasma membrane. In contrast, cones have cone-shaped outer segments, with disks continuous with the plasma membrane and exposed to the extracellular environment. The human retina has a single type of rod that uses the photopigment rhodopsin and three cone photoreceptor subtypes containing opsins sensitive to red, green, or blue wavelengths of light.

The retina is a highly ordered tissue of which photoreceptors form the layer furthest from incoming light, their outer segments directed toward the supporting retinal pigmented epithelium (RPE). Although outer segments undergo constant renewal by shedding disks distally and synthesizing new disks proximally, the structure and size

of photoreceptors is highly consistent across the retina and over time.[2] Thus, control over cell shape and size is required both developmentally and for ongoing cell maintenance. The mechanism of disk formation, only recently resolved, involves evagination of the plasma membrane at the base of the outer segment, followed in rods by engulfment of the disks within the plasma membrane.[7–9]

Here, we used zebrafish to study photoreceptor development and regulation. Aside from its advantages as an experimental model, zebrafish also have excellent color vision mediated by red, green, blue, and UV-sensitive cones.[10,11] Because both cones and rods are present in significant numbers, the zebrafish retina is ideal for comparing the factors that drive cone and rod development and maintenance.

What does it take to build and maintain an outer segment? As outer segments are modified primary cilia, the same basic machinery used in cilia formation is required for outer segment growth and photoreceptor survival.[12] Ciliopathies such as Bardet-Biedl, Joubert, Senior-Løken, and Meckel-Grueber syndromes typically include retinal dystrophy, but retinal ciliopathies can also be nonsyndromic.[13] In addition, ciliary growth and maintenance requires use of the intraflagellar transport machinery, and mutations in intraflagellar transport genes lead to photoreceptor degeneration.[5,14] However, to become efficient light-detecting sensors, outer segments have also developed many unique adaptations, including the components needed for creation and stabilization of the disks. For example, primary cilia typically release ectosomes containing signaling molecules, but in photoreceptor outer segments, ectosome release is blocked by the disk boundary protein Peripherin/Rds and disks are formed instead.[15]

The outer segments are densely populated with proteins that are required for phototransduction, but can also have a structural role. The best characterized is rhodopsin: preventing the transport of rhodopsin into the rod outer segment impedes outer segment growth and leads to photoreceptor degeneration.[16,17] Further, the level of rhodopsin gene expression is proportional to the outer segment volume.[18] Photoreceptor health depends on outer segment growth, but also on degradation of shed outer segment disks. Dysfunction of RPE, the tissue responsible for phagocytosis of shed disks, typically leads to photoreceptor death.[19]

Although many, but certainly not all, of the genes essential to photoreceptor survival have been identified, the factors that regulate photoreceptor size and morphology are less clear. And yet, each subtype of photoreceptor has a very defined structure across the retina and across species. Growth differentiation factor 6a (Gdf6a) is a morphogen expressed in the dorsal zebrafish optic cup, where it acts near the top of a hierarchy of factors patterning the dorsal retina. The loss of Gdf6a leads to microphthalmia, increased apoptosis, loss of dorsal markers, expansion of ventral markers, axonal misrouting, and two forms of coloboma.[20–26] Further, human *GDF6* mutations are associated with microphthalmia, coloboma, and the photoreceptor dystrophy Leber congenital amaurosis.[24,27,28]

Despite the many abnormalities of zebrafish *gdf6a* mutant eyes, the retinas are properly organized into three layers, and contain all expected cell types.[24] Previous research demonstrated an association between Gdf6 and photoreceptor degenerative disease, but no mechanism was uncovered.[28] Here, we use *gdf6a* mutants as a model to study photoreceptor maturation. We demonstrate how zebrafish eyes that develop in the absence of functional Gdf6a exhibit:

(1) short cone photoreceptors, (2) dysmorphic rod photoreceptors with expanded outer segments, and (3) a progressive overgrowth of the RPE. Using this system, we performed a transcriptome analysis to generate a cohort of factors that are candidate regulators of photoreceptor maturation.

METHODS

Zebrafish Husbandry and In Situ Hybridization

Zebrafish were cared for according to standard protocols, with animal ethics protocols approved by the University of Alberta Biosciences Animal Care Committee (AUP1476). Embryos and larvae were grown in embryo media at 28.5°C and staged appropriately. After 5 dpf, larvae were transferred to an aquatics facility and grown under 14:10 hour light/dark conditions. Transgenic strains were used to visualize rods [*Tg(-3.7rho:EGFP)kj2*][29] and UV cones [Tg($-5.5opn1sw1:EGFP)kj$].[30] Some of the UV transgenics also carried a transgene driving mCherry in blue cones [*Tg(-3.2opn1sw2:mCherry)mi2007*].[31] Alternative gene names for these opsins are *sws1=opn1sw1*, *sws2=opn1sw2*, and *rh1=rho*.[32] The *gdf6a*[s327] mutation encodes a S55X truncation producing a 54 amino acid peptide lacking the mature domain.[22]

Cryosectioning and Immunofluorescence

Whole larvae or enucleated eyes were fixed in 4% paraformaldehyde, washed three times in PBS (10 minutes) and sunk in 17.5% sucrose/PBS, followed by 35% sucrose/PBS for a minimum of 1 hour. The tissue was then embedded in Optimal Cutting Temperature media (Fisher Scientific, Hampton, NH), frozen on dry ice, and stored at –80°C. Sections (12 μM) were cut on a Leica cryostat and collected on Superfrost Plus (Fisher Scientific) slides. Slides were washed in PBS with 0.5% Tween and incubated in blocking solution containing 2% goat serum and 2 mg/mL BSA in PBS with 0.5% Tween. The following primary monoclonal antibodies were used: ZO1-1A12 (1:10, ThermoFisher Scientific, Waltham, MA), Zpr-1 (anti-Arr3a, 1:100), Zrf-1 (1:50), and Zs-4 (1:20). Zpr-1, Zrf-1, and Zs-4 were made by the University of Oregon Monoclonal Antibody Facility and obtained through the Zebrafish International Resource Center. Zpr-1 labels Arr3a and is a marker for red/green cones in zebrafish. TO-PRO-3 (1:1000; ThermoFisher Scientific) or propidium iodide were used for counterstaining of cell nuclei. After washing, slides were incubated at room temperature for 2 hours in goat anti-mouse Alexa Fluor 488 or 555 secondary antibody (1:1000; Molecular Probes, Eugene, OR). In some cases, Alexa Fluor 488-phalloidin (Molecular Probes) was applied with secondary antibodies at 1:100. All tissue was washed four times for 10 minutes in PBS with 0.5% Tween after primary and secondary antibody incubations. Slides were mounted in Aquapolymount (Polysciences, Inc, Warrington, PA).

Tissue Bleaching and Immunostaining for Rod Analysis

Tissue sections obtained from 5, 7, and 14 dpf control and *gdf6a* mutant zebrafish carrying the *rho:eGFP* transgene were bleached before immunostaining. The tissue was rehydrated in PBS and subsequently incubated in Coplin jars containing 10% H_2O_2/PBS at 55°C for 90 minutes. After bleaching, the slides or whole eyes were then rinsed

twice in PBS before proceeding with immunostaining. The tissue was incubated with a rabbit anti-GFP antibody (sc-8334; Santa Cruz Biotechnology, Santa Cruz, CA) at 1:100 overnight, followed by an Alexa Fluor 488 goat anti-rabbit secondary antibody (Molecular Probes, A11008) at 1:500 for 1 hour, and propidium iodide for 8 minutes (1:1000 dilution of 1 mg/mL stock, P4864; Millipore Sigma, Burlington, MA). Slides were mounted in Aquapolymount (Polysciences Inc) before imaging.

For whole *Tg(rho:eGFP)* larvae, bleaching was performed in microfuge tubes containing 10% H_2O_2/PBS at 55°C for 3 hours. After washing in PBS, larvae were immunostained as previously described,[33] with the same antibodies and stain as detailed above. Eyes were then removed and mounted in glycerol for imaging.

Paraffin Embedding

Zebrafish larvae were fixed in neutral buffered formalin fixative for a minimum of 48 hours. Positioning of the larvae was achieved by mounting in agar and then orienting the agar blocks into the paraffin wax molds. The fixed tissue was then transferred to 50% ethanol for 2 hours before going onto the tissue processor in 70% ethanol. The tissue was dehydrated in increasing ethanol washes before transfer to toluene and then wax. Larvae were embedded in paraffin to make blocks that were then sectioned at 5 μm on a microtome. The slides were dried at 37°C before staining.

Hematoxylin and Eosin Staining

Sectioned slides were first dewaxed with two toluene washes of 5 minutes, then a decreasing ethanol wash series (100%, 100%, 90%, 70%, and 50%) for 2 minutes each. Slides were washed in distilled water for 2 minutes before being stained with Hematoxylin Gill III for 2 minutes. After this, the slides were washed for 2 minutes in distilled water, then further rinsed under gently running cold tap water for 15 minutes. The slides were then put into 70% ethanol for 2 minutes before the eosin stain for 30 seconds. Two 100% ethanol washes followed by two toluene washes, each for 2 minutes, were then performed before coverslips were applied with DPX mounting medium.

Transmission Electron Microscopy

Zebrafish larvae were euthanized and then fixed overnight in 2.5% glutaraldehyde/2% paraformaldehyde in 0.1 M phosphate buffer. Samples were washed in 0.1 M phosphate buffer (3 × 15 minutes), treated for 1 hour with 1% osmium tetroxide in 0.1 M phosphate buffer, washed in 0.1 M phosphate buffer (3 × 15 minutes), and then gradually dehydrated through a series of increasing percentage ethanol solutions. Following three rinses in 100% ethanol, the tissue was treated for 1-3 hours in a 1:1 mix of ethanol and Spurr resin, and then put into pure Spurr resin overnight. After two more changes of Spurr resin, samples were embedded in flat molds and cured overnight at 70°C. Transverse sections of 70 to 90 nm thickness were cut with a diamond blade on a Reichert-Jung Ultracut_E Ultramicrotome and stained with uranyl acetate and then lead citrate stain. Imaging was performed on a Philips-FEI Morgagni 268 transmission electron microscope (FEI Company, Hillsboro, Oregon) operating at 80 kV and equipped with a Gatan Orius CCD camera (Gatan Inc, Pleasanton, CA).

RNA-Seq Sample Preparation and Analyses

Eyes were removed from anaesthetized *gdf6a* mutant (identified by microphthalmia) and sibling zebrafish larvae at 5 dpf after at least 30 minutes of light adaptation. For each sample, 125 eyes were collected from five clutches of larvae (25 eyes/clutch) and stored in RNAlater (Invitrogen, Carlsbad, CA) until processed for RNA extraction. The samples were collected on three different days from three separate breedings of *gdf6a* heterozygotes.

RNA extraction and RNA-Seq were conducted by The Applied Genomics Core at the University of Alberta. Total RNA from the zebrafish eyes was extracted with TRIzol Reagent (Life Technologies, Carlsbad, CA) according to manufacturer's protocol, and resuspended in 30 μL of RNase-free water, supplemented with 1 μL (40 U/μL) of RNAse-OUT (Life Technologies). One microgram of total RNA was used for preparation of RNA-Seq libraries using the TruSeq RNA Library Prep Kit v2 (Illumina, San Diego, CA), according to manufacturer's instructions. Libraries were quantified using a BioAnalyzer (Agilent, Santa Clara, CA) and a Qubit instrument (Life Technologies) and sequenced in a MiSeq instrument (Illumina) using a 75 cycles paired-end protocol that includes on-instrument demultiplexing at an approximate depth of 5.5 million paired-end reads per sample. Libraries were pseudo-aligned to draft GRCz10 of the *Danio rerio* cDNA database (Ensembl) with Kallisto.[34] Differential expression analysis at the level of transcripts was conducted with the R package Sleuth.[35] RNA-Seq data are publicly available at the SRA portal of NCBI under accession number PRJNA506585.

Quantitative PCR (qPCR) Sample Preparation

RNA for each genotype (*gdf6a* siblings and *gdf6a* mutants) was isolated from three pools of 90 individual eyes (45 fish) dissected as described above at 5 dpf following at least 30 minutes of light adaptation. Samples were stored in RNAlater (AM7020; Ambion, Inc, Austin, TX) at 4°C until extraction. Total RNA was extracted from pools of eyes using the RNeasy Mini Kit (74104; Qiagen, Hilden, Germany) according to the manufacturer's instructions. Samples were homogenized in 600 μL of Buffer RLT containing 1% of β-mercaptoethanol (M108; Sigma, St Louis, MO) with a rotor stator homogenizer and put through an on column DNAse digestion using Qiagen DNAse I (Qiagen, 79254). After Buffer RPE washes, RNA was eluted in 32 μL of molecular grade H_2O (Fisher Scientific, BP28191). RNA concentration and integrity were determined by running samples on an Agilent 2100 Bioanalyzer (Agilent RNA 6000 NanoChip).

cDNA Synthesis

RNA input was standardized to 350 ng per cDNA reaction. cDNA was generated using AffinityScript QPCR cDNA Synthesis Kit (Agilent Technologies, 600559) as per manufacturer's instructions. Each reaction consisted of 20 μL, with x μL of RNA (350 ng total RNA each reaction), 10 μL of 2× first strand master mix, 1.7 μL of oligo(dT) primers, 0.3 μL of random primers, and x μL of molecular grade water. cDNA was diluted 1:10 for qPCR experiments.

qPCR Parameters

The qPCR experiments followed MIQE guidelines[36] and were completed using a 7500 Real-Time PCR system

(ABI, Applied Biosystems, Foster City, CA) with 2× QPCR Mastermix (*Dynamite*, Molecular Biology Services Unit, University of Alberta). Transcript abundance was assessed relative to *rpl13a*, an endogenous housekeeping gene optimized for this experiment (see *Endogenous Control Assay*). Technical and biological replicates were performed in triplicate.

Endogenous Control Assay

To ensure *rpl13a* was a suitable endogenous control for qPCR, an endogenous stability assay was performed (see Fig. S7). Average C_t values were compared between three *gdf6a* sibling and three *gdf6a* mutant pools of eyes and were not significantly different. C_t values between both genotypes ranged from 16.53 to 17.09 (average, 16.791 ± 0.05). Each biological replicate ($n = 90$ fish eyes) was tested in triplicate.

Primer Validation

The qPCR primers were designed using Primer Express 3.0 in Geneious R9.1.7 software (Geneious, Auckland, NZ) and validated with a standard serial dilution to determine efficiencies. Primers were designed at the end of the 3′ exon in each gene or the 3′ untranslated region and were expected to amplify all splice variants. Primer sequences and efficiencies are available in Table S1, where a value of approximately 98% indicates the amplification efficiency of the target is approximately equal to the amplification of the reference.[37] Efficiencies were determined using Applied Biosystems 7500 Software v2.3 (Applied Biosystems). Disassociation curves were analyzed, and only primers producing a single peak were used.

Statistics

For all experiments, a Welch's *t*-test was calculated using an Excel plug-in created by Gaetano.[38] Boxplots were made using GraphPad Prism (Version 7.02 for Windows, GraphPad Software, www.graphpad.com).

Photography, Image Processing, and Analysis

Fluorescent images were taken with a Zeiss LSM 700 laser-scanning unit on a Zeiss Axioimager Z1 compound microscope (Carl Zeiss, Jena, Germany), with image processing done using the ZEN software (Zeiss) and Adobe Photoshop (Adobe, san Jose, CA). Differential interference contrast (DIC) images were taken on an Axiocam HR digital camera mounted on a Zeiss Axioimager Z1 compound microscope.

All *gdf6a* mutant eyes were included for analysis unless the entire retina was disorganized and in the process of degenerating, as seen in the subset of adult fish (28 dpf+) with pigment overgrowth. Only central tissue sections (those containing lens tissue) were selected for imaging. For the analysis of individual cells, z-stacks were taken and three-dimensional projections were created in order to select cells for analysis based on the following criteria: the cell was well aligned with the plane of the tissue section, was fully embedded within the section (i.e., had not been truncated by the sectioning), and had not been damaged (torn) by the sectioning. Cones were analyzed within the central 50% of the retina, while younger cells on the periphery were excluded (those within approximately 25% of the photoreceptor layer on either side). Measurements of length were made using

the open polygon tool in ZEN and tracked along the central contour of the cell (i.e., the line would turn if the cell was bent). Zpr1-labelled red/green cones were measured from the base of the cell body to the apex of the inner segment. UV cone length was measured from the base of the cell body to the apex of the outer segment. UV cone outer segment length was measured from just above the mitochondrial cluster in the ellipsoid region of the inner segment to the apex of the outer segment. Because most rods are peripheral, only the rods on the peripheral-most edges were excluded from analysis. Rod inner segment length was measured from the apical side of the cell body to (and including) the ellipsoid region. Rod outer segment length was measured from (and excluding) the ellipsoid region to the apex of the outer segment. In all rod and cone measurements, the axon and synaptic pedicle were excluded. UV cone and rod outer segment area measurements were made using the closed polygon tool in ZEN to outline the outer segment. Rod inner segment width was measured at the narrowest region of the myoid and widest region of the ellipsoid. See Figure S1 for example measurements and Table S2 for measurement data.

RESULTS

Cones in *gdf6a* Mutants have Reduced Apical Domains

Homozygous *gdf6a* mutant zebrafish embryos have a consistent microphthalmia phenotype apparent from 2 days post fertilization (dpf).[20,22] However, when the fish are grown to adulthood, the fate of the eyes is variable. Some of the mutants maintain small (approximately 50% of wild-type diameter), but otherwise normal-looking eyes, while in other individuals the eyes completely degenerate. Many of the fish have coloboma or small pupils, and the phenotypes can be unilateral or bilateral (Fig. S2). Previous work suggested that photoreceptors are specified normally in the absence of Gdf6a (*out of sight* mutant), although gaps are sometimes present in the photoreceptor layer.[24] The red/green cones of homozygous *gdf6a* mutants were observed to be reduced in size by 14 dpf and lost by adulthood.[28] However, given the variable phenotype of the adult eyes, we decided to analyze the photoreceptor changes systematically across all developmental stages.

We followed the development of red/green double cones and UV cones using two different markers. The antibody Zpr1 binds to Arrestin 3a and labels the red/green cones from the synaptic pedicle to the apex of the inner segment, but does not efficiently label the outer segment. UV-sensitive cones were visualized with the transgene *sws1:eGFP*, which facilitates examination of the entire cell morphology. At 4 dpf, the red/green cones were indistinguishable between the control (sibling) and *gdf6a* mutant retinas (Fig. 1). The photoreceptor layers were continuous and the cones had similar sizes and morphologies between mutants and sibling controls. The red/green cones were still comparable at 7 dpf, although any outer segment phenotype may be masked by the lack of labeling. By 14 dpf, we observed a significant size difference in Zpr1-labelled cells between mutant and control retinas, as reported previously (Fig. 1B).[28]

The UV cones showed a similar phenotype, with the cells differentiating normally, but subsequently failing to grow to the same extent as the UV cones in the control fish (Fig. 2). With the *sws1:eGFP* transgene, we could visualize the outer segment and more precisely determine the stage at which
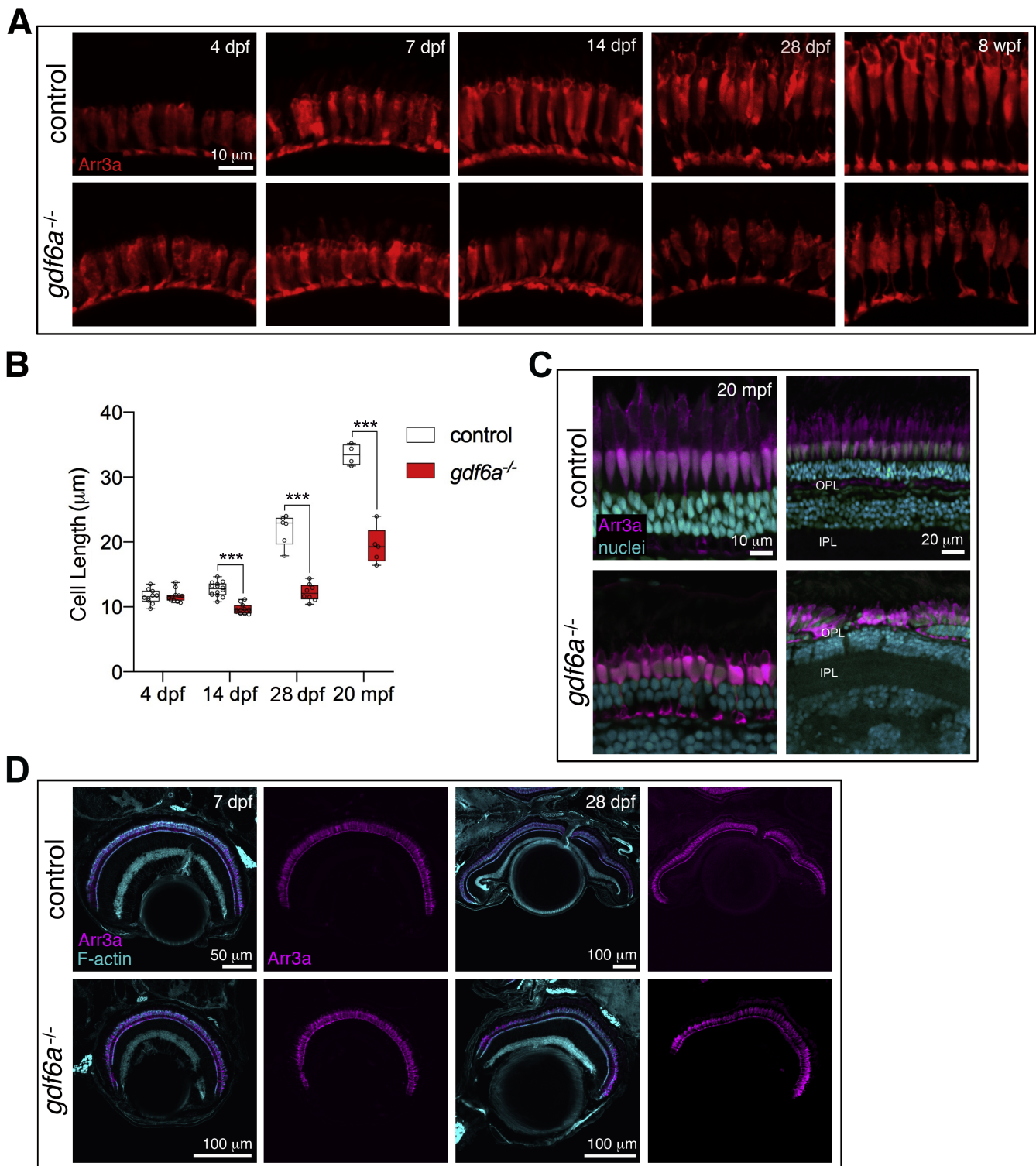
FIGURE 1. Morphology of red/green cones in *gdf6a* mutants. (**A**) Red/green cone morphology was evaluated by anti-Arr3a (Zpr1) immunostaining from 4 dpf to 8 wpf. The cones were indistinguishable at 4 and 7 dpf, but clearly smaller in the mutants by 14 dpf. (**B**) Measurement of the red/green cones from base of the cell body to apex of the inner segment showed a statistical change at 14 dpf, 28 dpf, and 20 mpf. Datapoints are average length of Zpr1-labelled cells for individual eyes. Measurements were made from base of cell body to apex of inner segment, with a minimum of three cells measured per eye. Error bars are SEM. ***$P < 0.001$. (**C**) The adult *gdf6a* mutants have intact red/green cones that continue to exhibit a smaller morphology than in the controls. One of the analyzed adult mutants had a patch of aberrant photoreceptors (*bottom right*). (**D**) The red/green cones form a continuous layer in the mutants, as shown at 7 dpf and 28 dpf. wpf, weeks post fertilization; mpf, months post fertilization.
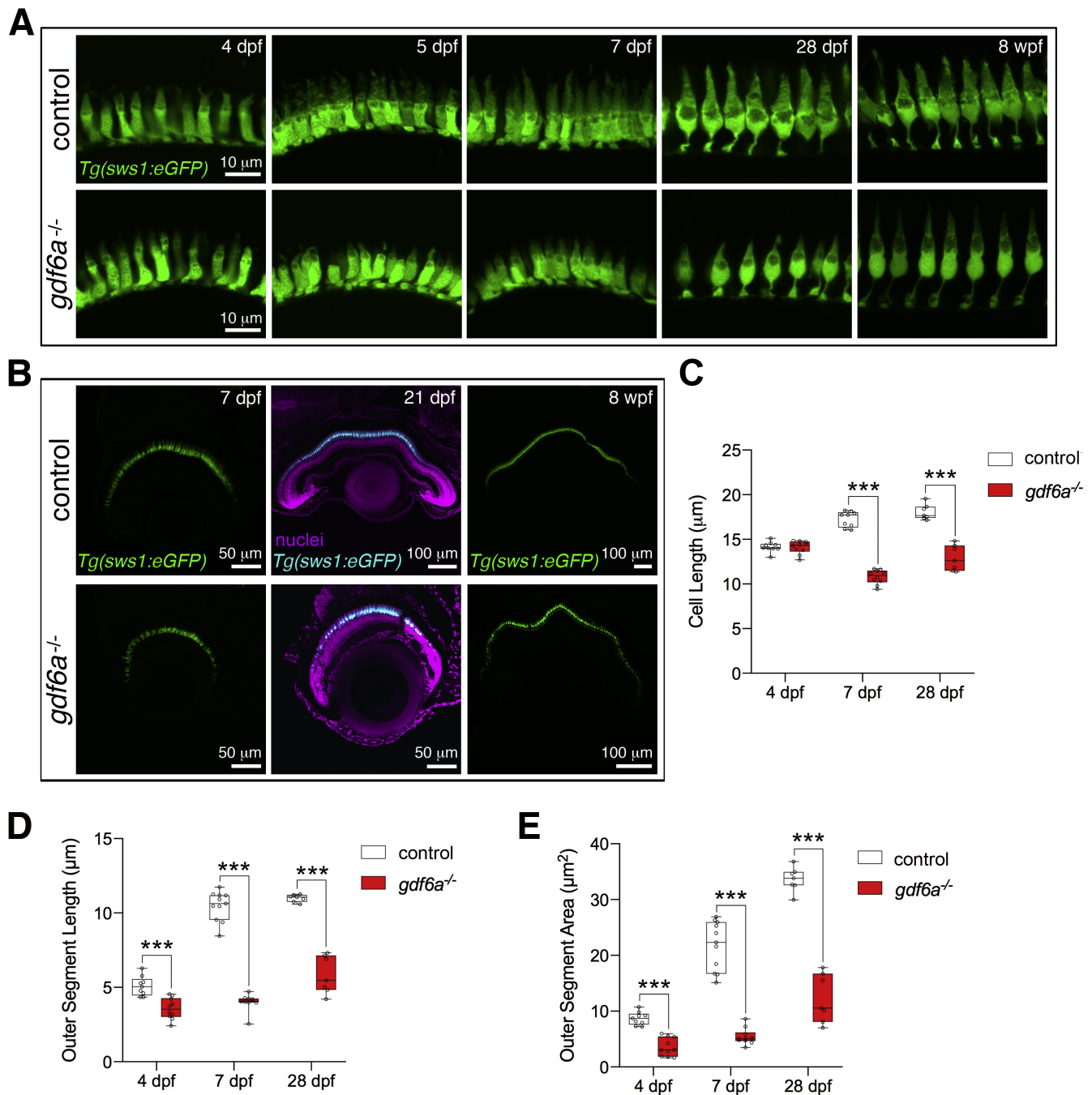
FIGURE 2. UV-sensitive cones have reduced outer segments in *gdf6a* mutants. (**A**) UV-sensitive cones visualized by the *sws1:eGFP* transgene appear similar between the *gdf6a* mutants and sibling controls at 4 dpf, but are noticeably reduced in size in the mutants at 5 dpf and at least up to 8 wpf. (**B**) UV cones form a continuous layer in the *gdf6a* mutant retinas at all ages examined. (**C**) Quantification of UV cone size, measured from base of cell body to tip of outer segment showed no difference at 4 dpf, but significant reduction at 7 and 28 dpf in the mutants. (**D**, **E**) Analysis of outer segment length and area revealed that the UV cone outer segments are already reduced in size at 4 dpf. Data points are average measurements for individual eyes, with a minimum of seven cells measured per eye. Error bars are SEM, ***P < 0.001; wpf, weeks post fertilization.

the mutant and wild-type cells diverged. At 4 dpf, the UV cones in control and *gdf6a* mutant larvae showed no significant difference in overall cell length (as measured from the base of the cell body to the apex of the outer segment). However, the 4 dpf mutants already had underdeveloped outer segments, as quantified by measurements of outer segment length and area. By 5 dpf, the UV cones in the

mutants were noticeably underdeveloped compared with controls, with significant differences in overall cell length, outer segment length, and outer segment area.

Based on the initial hypothesis that the cones are smaller because they are in the process of deteriorating and would soon be lost, we followed UV and red/green cone development over subsequent stages (Figs. 1 and 2). Unless the

entire eye was degenerating (as occurred in a subset of adults [Fig. S2] with small, pigment-covered eyes), *gdf6a* mutant retinas exhibited a layered organization and intact photoreceptors at all ages examined. From 14 dpf, red/green cones were consistently shorter in the *gdf6a* mutants, as quantified at 14 dpf, 28 dpf, and 20 months after fertilization (Fig. 1B), and yet the cells still exhibited distinct red/green cone morphologies. UV cone outer segment size and overall cell length were also significantly reduced at 14 and 28 dpf despite having the characteristic positioning and morphology of UV cones. In *gdf6a* mutant fish grown to 8 weeks after fertilization, the outer segments remain shrunken (Fig. 2A). Although blue cones were not examined in detail, we did observe in *gdf6a* mutant fish with mCherry-expressing blue cones a similar underdeveloped appearance from larval to adult stages (Fig. S3). In summary, the data support a model in which the cones in the *gdf6a* mutants are decreased in size, not because they are in the process of degenerating, but rather because regulation of their size is somehow altered.

Rods in *gdf6a* Mutant Larvae have Dysmorphic Inner Segments and Expanded Outer Segments

Rod morphology was visualized with another transgene (*rho:eGFP*) and analysis of larval retinas revealed abnormal rods in the *gdf6a* mutants (Fig. 3). At this stage, a rod inner segment in the control fish already consists of a thin myoid portion capped by an expanded ellipsoid region underlying the growing outer segment. The rods in the *gdf6a* mutants, however, have dysmorphic inner segments of inconsistent shape, with a notable expansion in width of the myoid region.

To better visualize the rod outer segments, we bleached the *Tg(rho:eGFP); gdf6a* mutant and control cryosections and subsequently immunostained for GFP (Fig. 3A). Surprisingly and in contrast with the cone phenotype, the rod outer segments in the *gdf6a* mutants grew robustly. Although less organized than in controls, the mutant rod outer segments were in fact visibly expanded by 5 dpf. The widened rod myoid regions, expanded rod outer segments, and shrunken cone outer segments in the 5 dpf *gdf6a* mutants can be simultaneously viewed in hematoxylin and eosin-stained paraffin sections (Fig. 3A, right column).

We did further imaging and quantification at 7 dpf, confirming a significant increase in rod outer segment length and area, with an associated reduction in inner segment length (Figs. 3B, C). We also noted a tendency of the rod outer segments to be bent and aligned almost perpendicular to the inner segment. In some cases, the cell would form a protrusion on the opposite side of the bend (inset image in Fig. 3B). Aside from the expanded outer segments, the arrangement of rods within the photoreceptor layer looked comparable between controls and mutants (Fig. 3B, middle column). However, to view the overall organization of the rod outer segments, some of the eyes were bleached, immunostained, mounted as wholemounts, and then imaged orthogonal to the plane of the cryosections (Fig. 3B, right column). The control rod outer segments are arranged in an orderly manner, with intervening space that would presumably be filled with cone outer segments. In contrast, the expanded and bent rod outer segments in the *gdf6a* mutants create a disorganized interlocking appearance.

As development progressed, the rod morphology partially recovered (Fig. 4). By 14 dpf, the control rod outer segments have grown considerably and are no longer significantly smaller than the *gdf6a* mutant rod outer segments. However, the mutants rod outer segments are still often bent and generally less organized than the controls (Fig. 4A). The inner segments in the mutants are variable, with some now appearing similar to controls. On average, though, the inner segments of the 14 dpf mutant rods are still expanded in width in the myoid region and decreased in length (Fig. 4C).

By 6 weeks, although the rod layer remained intact in the *gdf6a* mutants, the rods were highly variable in size between different mutant eyes (Fig. 4D), perhaps reflecting that some of the eyes were beginning to degenerate. The rod myoid regions had recovered in structure, now thin and indistinguishable between control and mutants, but the thickness of the inner segment layer was still significantly decreased in the mutants (Fig. 4E). The average thickness of the rod outer segment layer was not significantly different between controls and mutants.

Photoreceptor Ultrastructure and Layering in *gdf6a* Mutants

The abnormal growth of the *gdf6a* mutant photoreceptors could suggest internal disorganization of the cell. We therefore analyzed thin tissue sections by transmission electron microscopy at 5 dpf, when mutants exhibit cone under development and rod outer segment overgrowth, and again at 14 dpf, when the rods showed partial recovery (Fig. 5). At both ages, we observed cones in the *gdf6a* mutants that were well-formed, but had small outer segments. At 5 dpf, we could identify rods with expanded outer segments and wide inner segment myoid regions.

Although their morphology is abnormal, the rods and cones appeared healthy in the *gdf6a* mutants, with normal dense clusters of mitochondria in the apical inner segment and no evidence of cell fragmentation. Further, the membranous disks of the rod and cone outer segments in the *gdf6a* mutant larvae were properly organized without any inclusions, breaks, or disorganization at either 5 or 14 dpf.

One noticeable difference between the control and mutant retinas was the layering of the photoreceptors. As expected from previous work,[39] the UV sensitive cones form a distinct layer in 5 dpf control retinas, with their inner/outer segment boundary positioned basal to those of all other photoreceptor subtypes (Figs. 5A, S4). In the mutants however, the rod outer segments were most basal and the cone subtypes were not divided into distinct layers. By 14 dpf, the differences in positioning resolved and the photoreceptors were organized in the expected layers in both controls and mutants (Fig. 5B).

Comparative Transcriptomics Reveals Divergent Rod and Cone Gene Expression Changes

Our histologic analysis revealed that the *gdf6a* mutant larvae have a unique phenotype, whereby the cones have shrunken outer segments and the rods form expanded outer segments. Therefore, we decided to use these fish as a model to identify factors that potentially regulate outer segment growth in cones and rods, while also searching for the connection between loss of an early dorsal patterning gene and later disruption of photoreceptor maturation. We conducted RNA-Seq on isolated eyes from mutant and sibling larvae at 5 dpf,
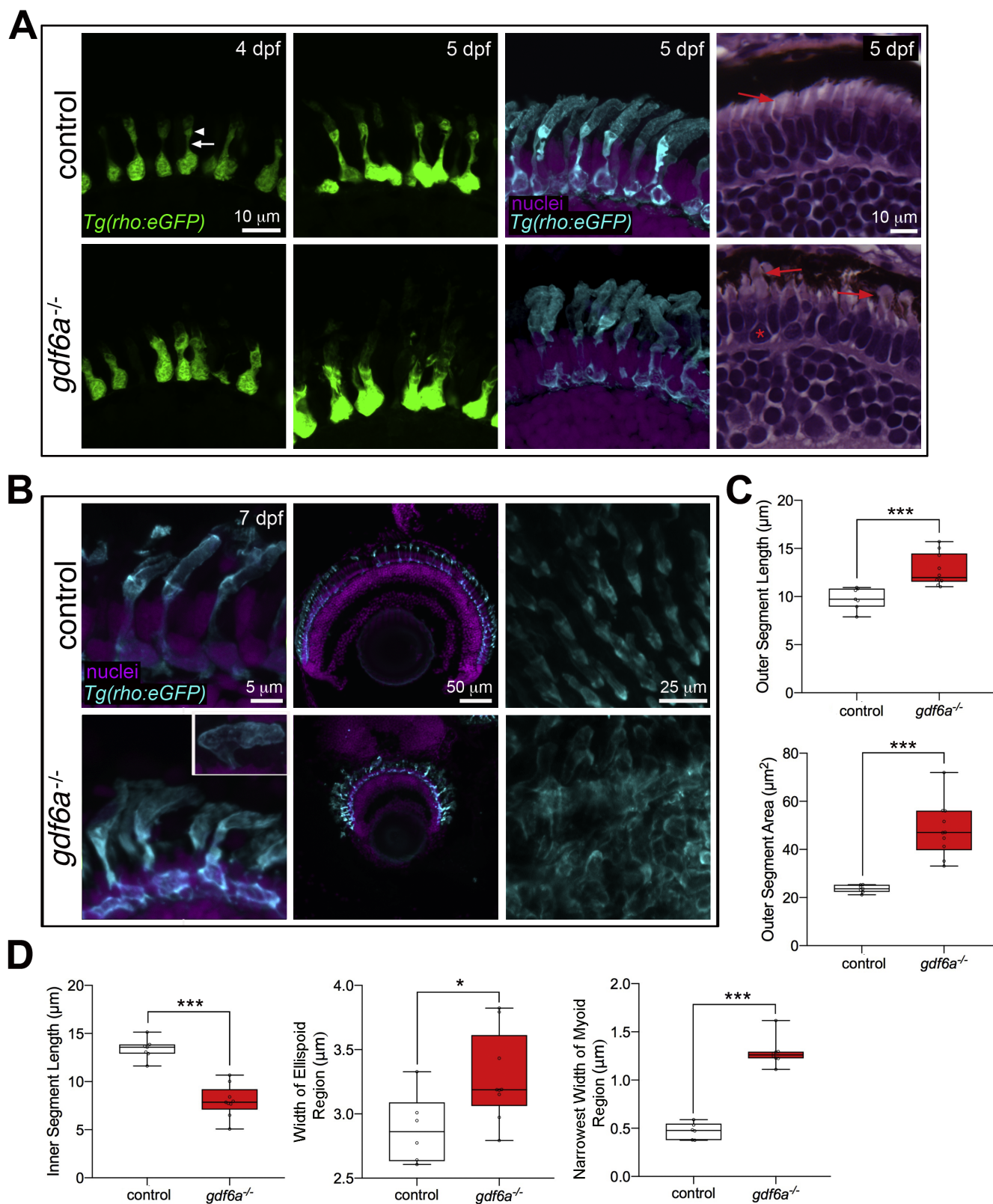
Figure 3. Rod morphology in *gdf6a* mutants. (**A**) Rods are initially dysmorphic in the retinas of larval *gdf6a* mutants. (**A**) Rods, as visualized by the *Rho:eGFP* transgene soon after differentiation (4 dpf, *left*). In controls, the myoid region (*arrow*) of the inner segment is already much thinner than the cell body, before expanding into the ellipsoid region (*arrowhead*) just below the outer segment (*top left*). In the *gdf6a* mutants, the myoid region is wider and more variable (*bottom left*). At 5 dpf, the inner segments remain abnormal. To better visualize the outer segments, 5 dpf sections were bleached to remove the pigment in the RPE and then immunostained for GFP (*third column*). In the mutants, the rod outer segments are expanded and less organized than in controls. Expanded rod inner and outer segments are also visible in 5 dpf hematoxylin and eosin-stained paraffin sections (*right column*). *Red arrows* point to the rod outer segments and red asterisk marks a rod with a wide inner segment. (**B**) Rod morphology in *gdf6a* mutants and controls at 7 dpf. The outer segments remain expanded, but

are also often folded (inset, *lower right*). The rod photoreceptor layer is comparable between controls and mutants (*middle column*). Whole 7 dpf eyes bleached and immunostained for GFP were mounted with the lens down and imaged from above (*right column*). In the whole eyes, the rods in the controls appeared as a regular array, while the expanded and folded rod outer segments in the *gdf6a* mutants formed a disorganized interlocking layer. (**C**) Measurements of rod outer segment morphology revealed a significant expansion in outer segment length and area in the mutants. (**D**) Quantification of inner segment morphology shows that the inner segments are shorter, but expanded in width in both the myoid and ellipsoid regions. Each data point represents the average measurement for an individual eye, with a minimum of seven cells measured per eye. Error bars are SEM, *$P < 0.05$, **$P < 0.01$, *** $P < 0.001$.

a time-point when both rod and cone outer segment phenotypes are apparent.

Consistent with the small cone and enlarged rod outer segments observed in sectioned retinas, the RNA-Seq data showed profound and consistent changes in transcripts coding for outer segment proteins (Fig. 6, Table S3, Fig. S5). Using a stringent cutoff of a two-fold upregulation or downregulation plus statistical significance, we discovered that the vast majority of genes associated with the rod phototransduction pathway were upregulated, while the vast majority of cone phototransduction genes were downregulated, including all of the major opsins. The altered expression of rhodopsin and two of the cone opsins was confirmed by qPCR (Figs. S6 and S7). Of 187 significantly altered transcripts, 15 were upregulated rod-specific outer segment genes and 16 were downregulated cone-specific outer segment genes. One exception is the cone gamma transducin subunit *gngt2a*, which has two upregulated isoforms. However, the more highly expressed paralogous gene, *gntg2b*, is downregulated.

The genes *rom1a, rom1b, peripherin 2a* (*prph2a*), and *prph2b* encode proteins essential for the rim structure of outer segment disks. Although the genes are not expressed in a rod- or cone-specific manner, we did note that both *rom1* genes are elevated, while both *prph2* genes are reduced. Interestingly, experiments in mouse showed that the ratio of *rom1* to *prph2* is higher in rods than cones,[40] and so the expression changes may still be explained by the altered outer segment sizes.

Although the transcriptomic results are consistent with our analysis of the altered photoreceptor morphologies in the *gdf6a* mutants, it is important to consider whether the data may also be influenced by changes to relative numbers of the individual cell types within the eyes. We therefore searched the Zebrafish Information Network (zfin.org) for genes that could be used as markers for the retinal ganglion cell or outer nuclear layers at 4 to 5 dpf (Table S4). In addition to 9 genes expressed in the retinal ganglion cell layer, we identified 19 outer nuclear layer genes that do not encode outer segment proteins. In both cases, the data revealed a nearly equal mix of upregulated and downregulated genes, with only three genes showing a significant change (one retinal ganglion cell gene and two outer nuclear layer genes, all downregulated). This finding is in contrast with the consistent upregulation of rod outer segment genes and downregulation of cone outer segment genes, and argues against a change in the ratio of inner to outer retinal cell types.

Within the photoreceptor layer, specification of the various photoreceptor subtypes was previously analyzed in the *gdf6a* mutant larvae and no change was found in the ratio of rods to UV cones.[41,42] The authors did report decreases in the numbers of blue- and red-sensitive cones, but far less than could account for the 4.7 and 5.8-fold decreases in the blue (*opn1sw2*) and red opsin genes, respectively. Further, we detected no change in the ratio of red/green cones to rods in 5 dpf larvae (Fig. S8,

2.3 ± 0.4 for controls vs. 2.3 ± 0.5 for *gdf6a* mutants, $n = 3$ eyes for each), and we suspect that the previously reported reduction in red cones arose from the use of an outer segment antibody that would poorly label the underdeveloped cones in the *gdf6a* mutants. In summary, the RNA-Seq data are likely reflective of the dramatic alterations to outer segment morphology rather than of disrupted photoreceptor specification.

Inner Segment Gene Expression and Protein Localization

Although the microscopy data showed clear morphologic changes to the inner segments of both rods and cones, the RNA-Seq experiment did not reveal the same correlative gene expression changes as was found for the outer segments. For example, the ellipsoid region of the inner segment lies just below the connecting cilium and contains large assemblies of mitochondria.[3] In using the MitoMiner 4.0 interface to cross-reference our database of 187 significantly altered transcripts with the MitoTracker 2.0 database[43] of 1158 genes encoding mitochondrial-localized proteins, we identified only three genes (rpl6, hspb1, and cyb5a). Interestingly, all three were upregulated (Table S3, second tab).

Inner segments are also the site of localization for cell polarity factors such as Crumbs. The Crumbs transmembrane proteins are essential for establishing and maintaining apical polarity in a wide variety of epithelial cell types,[44] and mutations in human *CRB1* underlie a spectrum of severe retinal diseases.[45,46] The photoreceptor Crumbs domain begins at the intercellular adhesion junctions and then extends apically along the cortex of the inner segment.[47,48] In the zebrafish retina, *crb2a* is expressed in all photoreceptors, whereas *crb2b* is expressed in red, green, and blue cones,[48] and knockdown of Crb2b was reported to cause a small red/green cone phenotype similar to that seen in the *gdf6a* mutants.[49]

Immunolabelling of *gdf6a* mutant retinas with the Crb2a antibody Zs-4[47] revealed expression in the expected location just apical to the outer limiting membrane (OLM), the site of photoreceptor adherens junctions. However, the Crb domain was shortened in height in the mutants, a difference already obvious at the earliest stages of photoreceptor maturation (Figs. 7A, B). Notably, Crb2a is expressed in all photoreceptors[48] and therefore the consistent decrease in the length of the Crb2a domain implies similar changes in rods and cones, matching the observed shortening of inner segments for both types of photoreceptor.

The Crumbs domain is located within the myoid portion of the rod inner segment, the morphology of which was highly abnormal in the larval stage *gdf6a* mutants. Interestingly, the less affected mutant rods exhibited a characteristic bulge in the inferior portion of the myoid (Fig. 7A, bottom middle), a phenotype seen previously in zebrafish rods overexpressing wild-type Crb2b.[47]
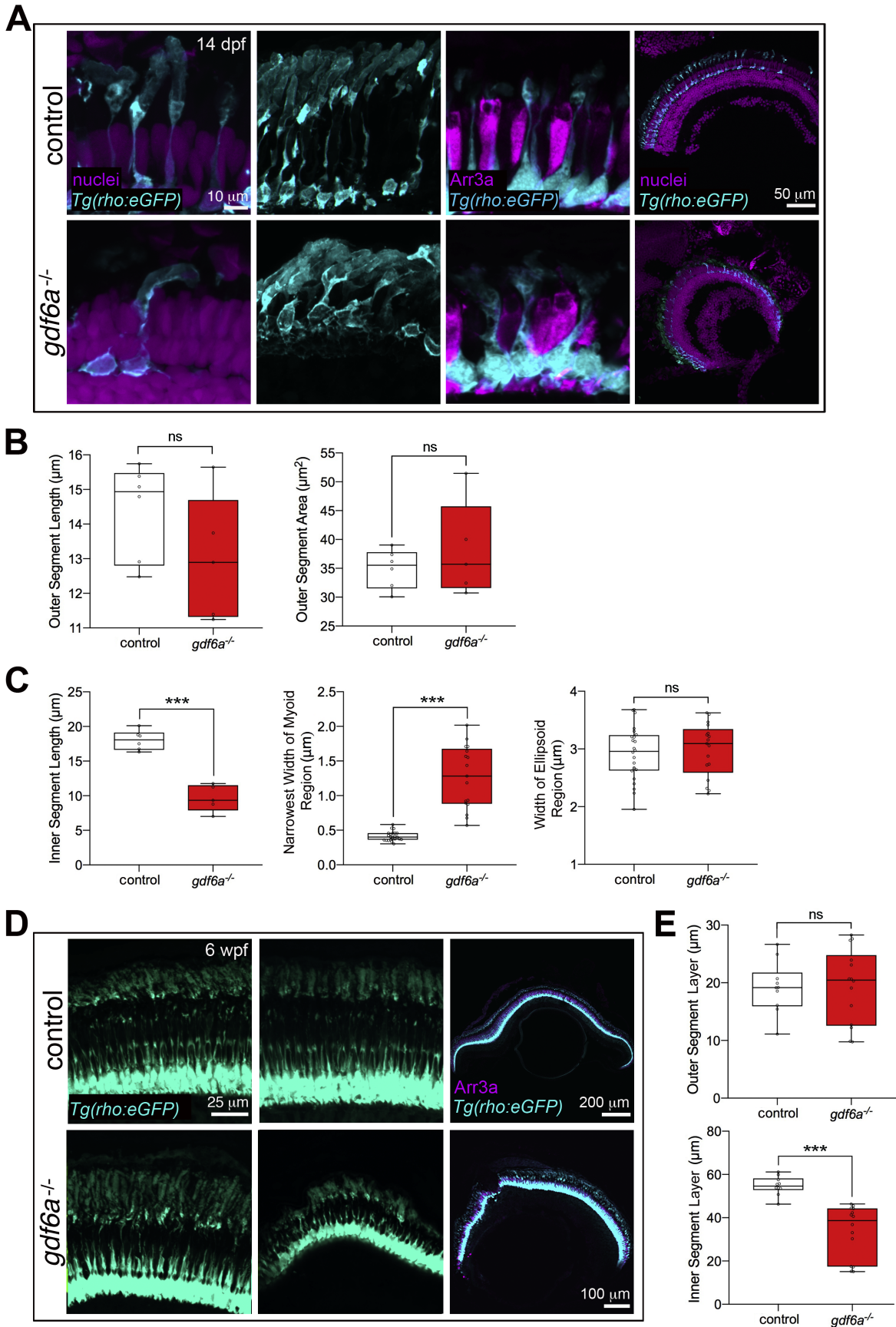
Figure 4. Partial recovery of rod morphology in older *gdf6a* mutants. (**A**) Rod photoreceptors in 14 dpf zebrafish. A rod in the central retina of a *gdf6a* mutant eye (*bottom left*) has a similar morphology to the rods in a control eye (*top left*), although the outer segment is bent. Rods

in the peripheral retina (*second column*) no longer have an expanded outer segment in the *gdf6a* mutants, although the cells are still more disorganized than in controls. The inner segments are variable, but on average remain shorter (*first and second columns*) and expanded in width (*third column*). (**B**) Quantification of outer segment morphology shows no significant difference in length or area between rods in controls and *gdf6a* mutants. (**C**) Quantification of the inner segment morphology, revealing that the rod inner segments in 14 dpf *gdf6a* mutants remain shorter and expanded in width in the myoid region (measured at the narrowest width), but are no longer expanded in the ellipsoid region. Data points are averages from individual eyes, with a minimum of seven cells measured per eye. (**D**) The size of the rods is variable in 6-week-old *gdf6a* mutant eyes, ranging from comparable with controls (*bottom left*) to severely shrunken (*bottom right*). The mutant eyes still have a complete rod photoreceptor layer (*right column*). (**E**) Quantification showing no significant difference in thickness of the outer segment layer, although there is high variability in the mutants, and the thickness of the inner segment layer remains reduced at 6 weeks. Each data point is the average of three measurements across the inner or outer segment layer for an individual eye. Error bars are SEM, *** $P < 0.001$. wpf, weeks post fertilization; ns, not significant.

In total, the *gdf6a* mutant photoreceptors show similarities to previously reported Crb gain- and loss-of-function phenotypes, and exhibit a reduced Crb domain. The RNA-Seq results were similarly inconsistent, with detected transcript levels of *crb2a* and *crb2b* being low and highly variable, showing no significant changes. This finding could suggest a change in localization or processing of the protein in the mutants, or the observed shortening of the Crb domain may simply be a reflection of the length of the inner segment. Notably, other known cell polarity factors such as *mpp5a* (nagie oko), *epb41l5* (mosaic eyes), and *prkci* (aPKC) similarly show no significant change in expression.

Although nearly absent from the outer segment, actin fibers are a prominent feature of the photoreceptor inner segment.[50] Phalloidin staining of F-actin revealed grossly normal organization of the actin fibers lining the cell cortex of the inner segment and radiating from the cell-cell junctions of the OLM in the *gdf6a* mutants (Fig. 7A), and the expression levels of the β-actin genes, *actb1* and *actb2*, were unchanged between mutant and sibling eyes. However, the actin fibers in the mutant rods did not extend as far in the apical–basal axis, consistent with shorter inner segments and reduced Crb2a domains in both cones and rods.

Interestingly, one downregulated inner segment gene was *kcnv2b* (33-fold in RNA-Seq, 32-fold in qPCR; Table S3, Fig. S6), which codes for the modifier potassium channel subunit Kv8.2 proposed to function as a regulator of dark current.[51] In humans, *KCNV2* mutations exclusively cause cone dystrophy with supernormal rod response,[50,51] a disease characterized by ERG recordings that feature a decrease and delay in scotopic response to dim flashes in both rods and cones, juxtaposed with a supernormal rod b-wave response to bright flashes.[54] The underlying cone dystrophy with supernormal rod response pathology is unclear, but the phenotype is of interest to us considering the observed expansion of the rod outer segments and reduction of cone outer segments in the *gdf6a* mutants. However, zebrafish have two *kcnv2* genes, and the rod-expressed *kcnv2a*[55] shows a significant and possibly compensatory upregulation (1.86-fold on RNA-Seq, 2.73-fold in qPCR).

Müller Glia and RPE

The *gdf6a* gene is expressed widely in the dorsal retina from the optic vesicle stage, but becomes restricted to the dorsal ciliary marginal zone (CMZ) by 48 hpf.[20,21] Notably, photoreceptor differentiation and the appearance of photoreceptor abnormalities in the *gdf6a* mutant eyes occur well after the broad Gdf6a expression has disappeared. In addition, the photoreceptor changes were not localized to the dorsal or ventral retina. Therefore, we hypothesized that the phenotype arises indirectly through the abnormal development of other cell types in the eye. In particular, photoreceptors are highly dependent on Müller glial and retinal pigmented epithelial cells.

Müller glial cells extend apical processes that form adherens junctions with the photoreceptor inner segments at a defined level, giving rise to the visible line of the OLM. Antibody staining of Müller glia revealed normal extension of glial processes across the width of the mutant retinas (Fig. 8A) and DIC imaging exposed a distinct OLM (Fig. 8B). The protein zonula occludens-1, although typically a marker of tight junctions, is a component of the photoreceptor–glial adhesions,[56] and zonula occludens-1 immunolabelling highlighted punctae present along the OLM in both control and *gdf6a* mutant retina. Further, F-actin is associated with the cytoplasmic face of the junctions[57] and labeling of F-actin fibers marked a clear OLM in both controls and mutants.

Although glial cells are a structural presence in the *gdf6a* mutant retina, there remains a possibility for functional impairment. For example, Müller glia recycle the bleached cone visual pigments.[58,59] However, blocking the cone visual cycle does not lead to altered photoreceptor morphology[60] and we did not detect any changes in the expression of glial-associated genes in our RNA-Seq analysis. In summary, disruption of Müller glia is unlikely to underlie the aberrant photoreceptor changes in *gdf6a* mutant fish.

A healthy RPE is also critical for maintaining the integrity of the photoreceptors.[19] The RPE forms a membrane barrier separating the photoreceptors from the choriocapillaris blood vessels, recycles bleached retinal molecules, and maintains an optimal extracellular environment in the outer retina. Photoreceptors constantly renew their outer segments by shedding distal membranous disks while making new ones proximally, and the RPE cells phagocytose and break down the shed disks. When photoreceptors become detached from the RPE, or if the RPE degenerates, death of the photoreceptors promptly follows. In the *gdf6a* mutants, the RPE forms a continuous layer without evidence of degeneration at 5 dpf, and RPE villi extend into the photoreceptor layer and surround the outer segments in the mature retina (Fig. 8C). Importantly, the appearance of abnormal cones and rods precedes the reported start of outer disk shedding at 6 dpf (unpublished observations cited in[47,61]) arguing against a defect in RPE phagocytosis as a primary driver of the photoreceptor changes.

Instead of displaying the RPE degradation common in numerous retinal dystrophies, many of the older *gdf6a* mutant fish exhibited overgrowth of pigmented cells in the anterior eye. By 4 weeks, some of the mutant fish had pigmented cells fully covering the lens or even growing between the lens and the retina (Figs. S2, 8C). Notably, an association was previously made between disruption of the
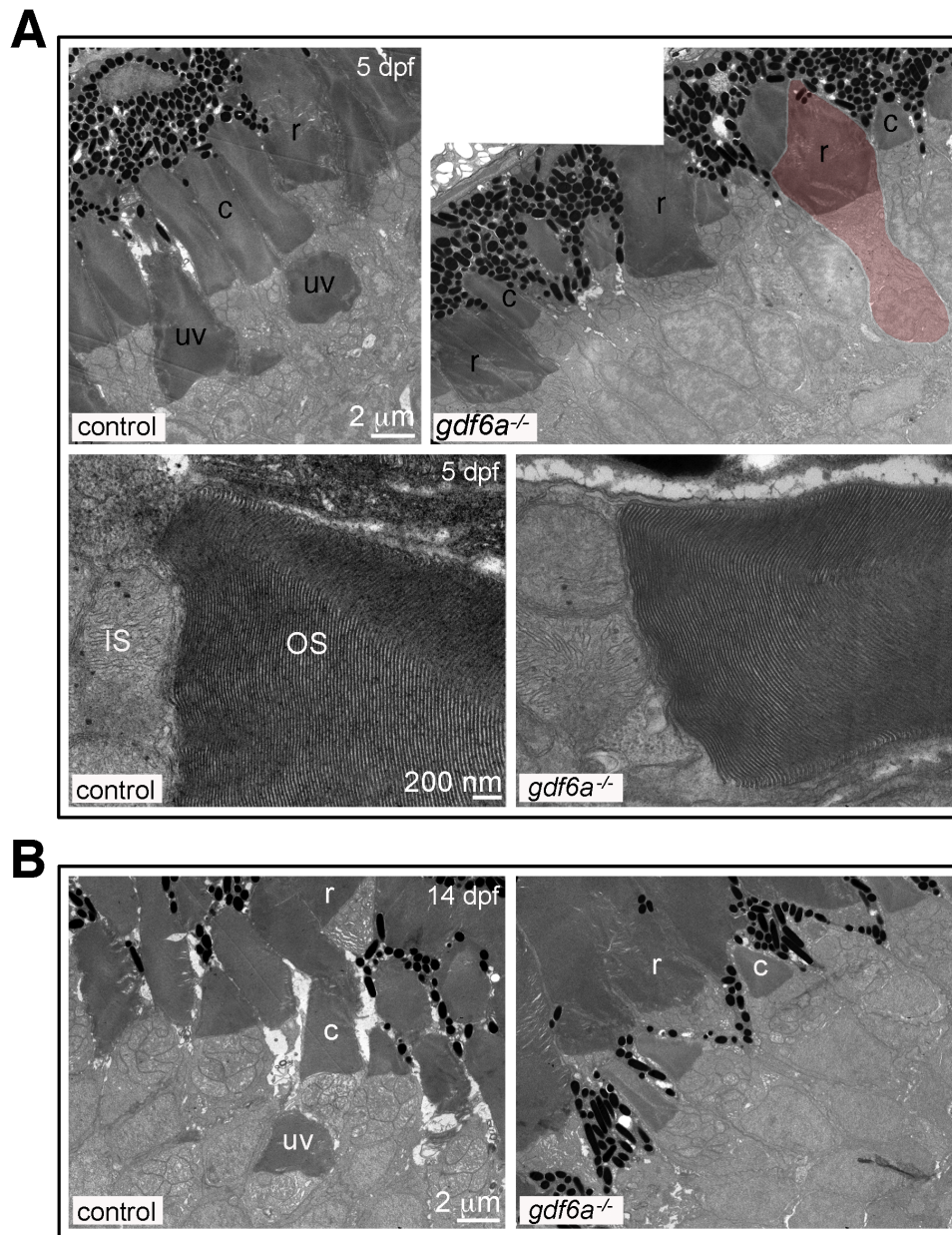
Figure 5. Photoreceptor ultrastructure in *gdf6a* mutants. (**A**, **B**) Transmission electron microscopy photographs of photoreceptors in control and *gdf6a* mutant zebrafish retinas. (**A**) At 5 dpf, the cone photoreceptors in the control retina (*top left*) have formed sizable outer segments present in two layers: a basal layer for UV-sensitive cones (uv) and an apical layer for the other cone subtypes (c). The rod outer segments (r) are closely associated with the more apically located cone outer segments. In the *gdf6a* mutants (*top right*), the cones have small outer segments (c) and are not separated into multiple layers. The rod have inner segments expanded in width (*red highlighted cell*) and capped by large outer segments (r) that ectopically begin basal to the cone outer segments. At higher magnification, the outer segment membranous disks are indistinguishable between photoreceptors in control and *gdf6a* mutant eyes at 5 dpf (*bottom row*). (**B**) By 14 dpf, the layering is resolved, with rod positioned apically and UV cones positioned most basally (Note: no UV cones are present in the right photo. See Fig. S4 for further images of UV cone positioning). Three control and three mutant retinas were analyzed at each stage.

proliferative CMZ and subsequent overgrowth of RPE in the anterior segment.[62] Genetic and proliferative changes in the CMZ of *gdf6a* mutants have been well characterized,[21,26] and our RNA-Seq analysis uncovered at least 10 misregulated CMZ genes as well as an increase in the retinoid metabolism genes expressed in RPE (Table S3, Fig. S5D). In summary, we did not find any deficits in RPE structure or function, but instead revealed RPE overgrowth at the retinal margin possibly occurring secondary to CMZ depletion.

Here, we have carefully documented the unusual maturation of photoreceptors in eyes lacking Gdf6a. Because *gdf6a* is not expressed in or near the differentiating photoreceptors[20] and did not appear as a significantly downregulated gene on the RNA-Seq, it is unlikely to have a direct role in late-stage photoreceptor development. Therefore, the altered photoreceptor morphology in the *gdf6a* mutants likely arises from one of two mechanisms: (1) early disruption of eye patterning in turn altering the signals needed for
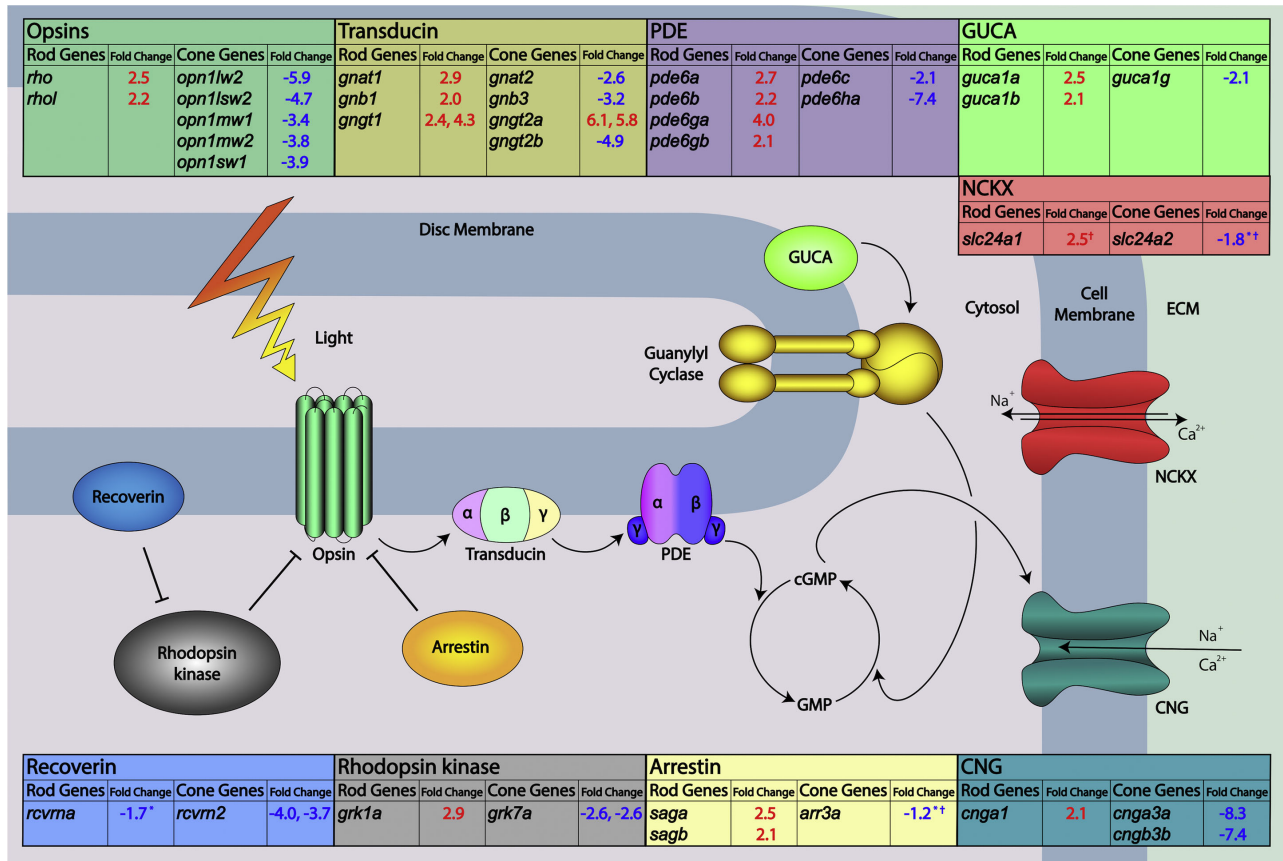
Opsins

Rod Genes	Fold Change	Cone Genes	Fold Change
rho	2.5	opn1lw2	-5.9
rhol	2.2	opn1lsw2	-4.7
		opn1mw1	-3.4
		opn1mw2	-3.8
		opn1sw1	-3.9

Transducin

Rod Genes	Fold Change	Cone Genes	Fold Change
gnat1	2.9	gnat2	-2.6
gnb1	2.0	gnb3	-3.2
gngt1	2.4, 4.3	gngt2a	6.1, 5.8
		gngt2b	-4.9

PDE

Rod Genes	Fold Change	Cone Genes	Fold Change
pde6a	2.7	pde6c	-2.1
pde6b	2.2	pde6ha	-7.4
pde6ga	4.0		
pde6gb	2.1		

GUCA

Rod Genes	Fold Change	Cone Genes	Fold Change
guca1a	2.5	guca1g	-2.1
guca1b	2.1		

NCKX

Rod Genes	Fold Change	Cone Genes	Fold Change
slc24a1	2.5†	slc24a2	-1.8*†

Recoverin

Rod Genes	Fold Change	Cone Genes	Fold Change
rcvrna	-1.7*	rcvrn2	-4.0, -3.7

Rhodopsin kinase

Rod Genes	Fold Change	Cone Genes	Fold Change
grk1a	2.9	grk7a	-2.6, -2.6

Arrestin

Rod Genes	Fold Change	Cone Genes	Fold Change
saga	2.5	arr3a	-1.2*†
sagb	2.1		

CNG

Rod Genes	Fold Change	Cone Genes	Fold Change
cnga1	2.1	cnga3a	-8.3
		cngb3b	-7.4

FIGURE 6. Altered expression of cone and rod-specific outer segment genes in *gdf6a* mutants. The figure shows all essential components of the phototransduction cascade and their associated transcriptional changes as detected by the RNA-Seq analysis of *gdf6a* mutant eyes compared with sibling controls at 5 dpf. Most transcripts coding for cone-specific phototransduction pathway components showed significant downregulation in the *gdf6a* mutants, while those coding for rod-specific phototransduction components were upregulated. All changes were statistically significant and above the two-fold change threshold unless marked. *A change of less than the two-fold threshold; †A change that is not statistically significant. ECM, extracellular matrix.
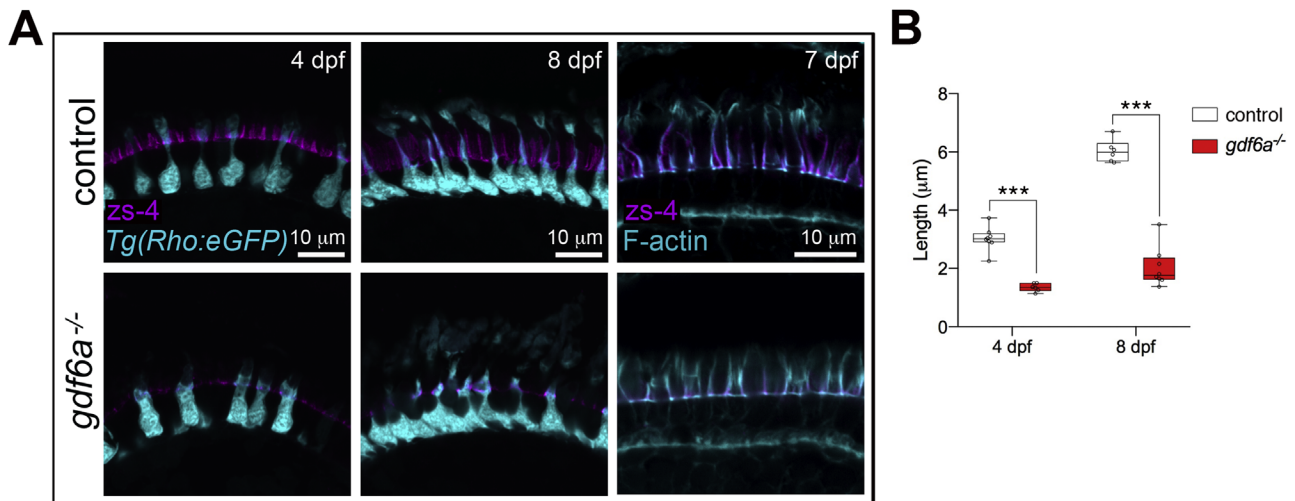
FIGURE 7. Reduced Crumbs domain in *gdf6a* mutants. (**A**) Crb2a (immunostained with the Zs-4 antibody) is localized properly in the photoreceptor inner segments of *gdf6a* mutants, but the domain is reduced in apical-basal extent. Actin fibers present in the inner segment are similarly shortened in the mutants (*third column*). (**B**) Quantification of the apical-basal length of the Crumbs domain; ***$P < 0.001$.

proper photoreceptor differentiation, or (2) changes to the structure of the eye or the supporting tissues secondarily disrupting the photoreceptor structure. In either case, gene expression changes within the photoreceptors must occur
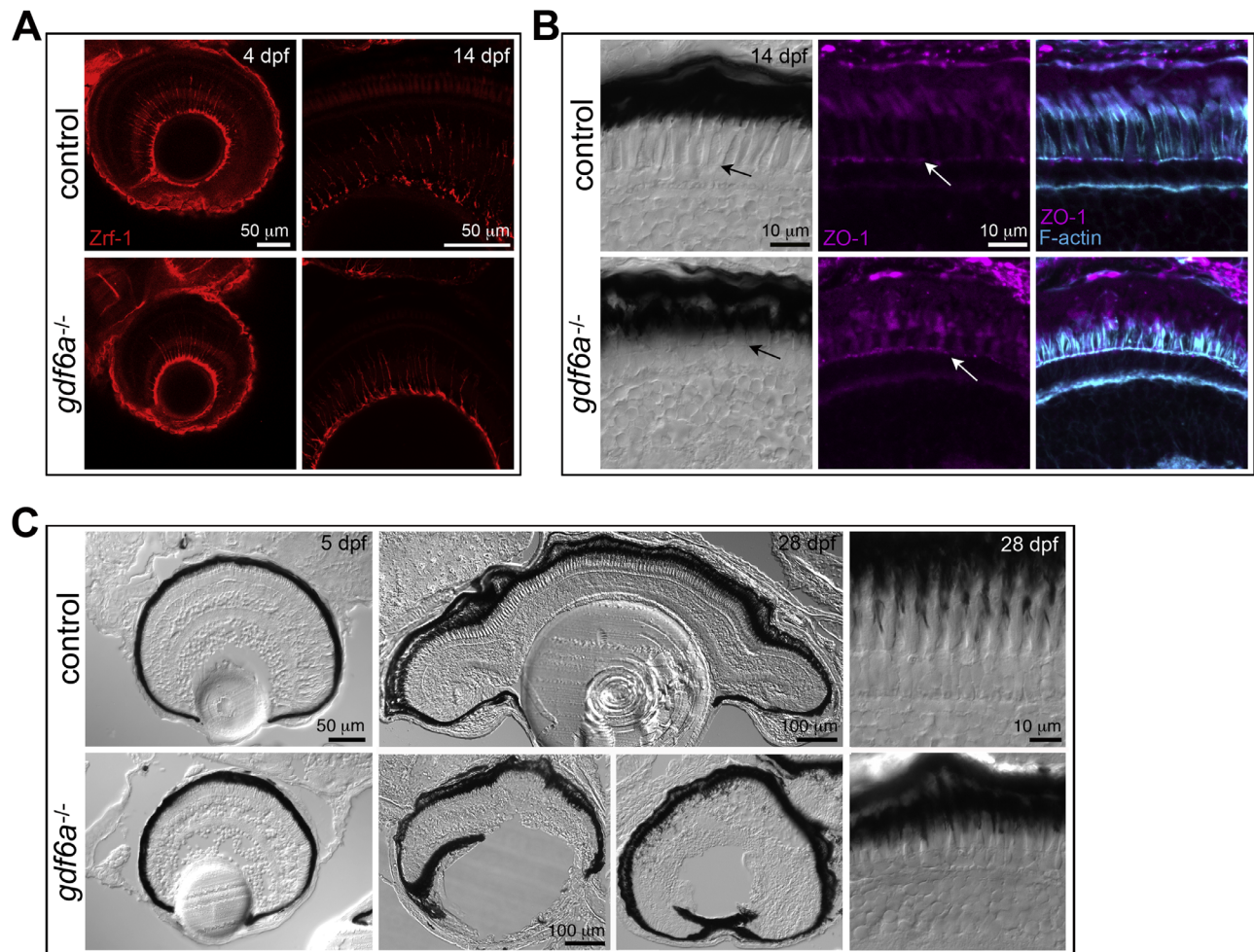
FIGURE 8. Müller glia and RPE in *gdf6a* mutants. (**A**) The Müller glia extend processes across the retina in control and *gdf6a* mutant retinas. (**B**) The OLM is visible in control and mutant retinas (*arrow*) in DIC images (*first column*) and through staining with the tight junction marker zonula occludens-1 (*second and third columns*) and for actin (*third column*). (**C**) The RPE initially forms a continuous layer in the mutant retina, without evidence of overgrowth or degeneration (*left*). By 28 dpf, many of the mutants display overgrowth of pigment cells in the anterior ocular segment, leading to spreading over the lens or between the lens and the retina (*center*). The RPE cells extend villi into the photoreceptor layers of both control and mutant retinas (*right*).

to support the distinct cell morphologies in the mutants. Indeed, the RNA-Seq dataset revealed a substantial cohort of misregulated genes, some of which are candidate drivers of the observed morphologic changes.

One example of a downregulated gene of interest is *tmem237a* (8.4-fold by RNA-Seq, Table S3; 5.59-fold by qPCR, Fig. S6). TMEM237 is part of the ciliary transition zone complex and mutations underlie cases of Joubert syndrome related disorders, which are ciliopathies with associated vision defects.[63,64] Aside from a proposed role controlling protein movement in and out of the outer segment as part of the ciliary gate, TMEM237 is also expressed in rod outer segments[64] and therefore may influence photoreceptor morphology in multiple ways.

DISCUSSION

The *gdf6a* mutants are functionally blind, as measured at 7 dpf by the optomotor response assay.[28] However, the reason for the blindness is unclear. Although small, the mutant eyes

have retinas with all the expected cell types arranged in proper order,[24] and we show here that the photoreceptors form outer segments with the correct layering of membranous disks. The visual deficits of *gdf6a* mutant fish likely arise from a combination of developmental defects, including coloboma, lens malformation, and disrupted axonal targeting,[20,22,24] as well as the malformed photoreceptors. Notably, we found that the fish are difficult to raise to adulthood because the vast majority die between 1 and 2 weeks post fertilization. At that stage, the fish are beginning to feed while entirely dependent on cone vision.[65] Interestingly, the mutant fish that do survive to 2 weeks, which is the onset of rod function, will typically go on to adulthood and are unperturbed by the introduction of live food.

The restriction of *gdf6a* expression to the dorsal CMZ by 48 hpf[20,21] argues against a direct role for Gdf6a in photoreceptor maturation and led to our initial hypothesis that the observed phenotypes arise from defects in associated cells, particularly the Müller glia or RPE. However, neither showed overt signs of degeneration or dysfunction, and the RPE instead later overgrew into the anterior segment. In addition,

the mutant photoreceptor phenotypes were apparent before the start of disk shedding and phagocytosis.[47,61] Nevertheless, the RPE and Müller glia play multiple important roles in maintaining photoreceptor function and health,[19,66] and it remains possible that functional changes could feed back to modify photoreceptor structure.

In a previous study, we characterized the abnormal development of the ocular vasculature in *gdf6a* mutant eyes.[23] An insufficient vascular supply would compromise the development of photoreceptors, the most metabolically active cells of the body.[67] Although we cannot discount the possibility, the data argue against such a mechanism. First, the widespread apoptosis in *gdf6a* mutant embryonic eyes occurs primarily before the vasculature is established or photoreceptors differentiate.[21] Second, we did not observe in the small mutant eyes any evidence for hypoxia, such as upregulation of hypoxia-inducible factors or buildup of lipid droplets in the RPE (Table S3, Fig. 5A).[68] Third, instead of the photoreceptor degeneration that occurs secondary to hypoxia in age-related macular degeneration,[69] we demonstrated here how *gdf6a* mutant eyes generate an uninterrupted photoreceptor layer that can be maintained into adulthood, although we cannot discount a slow turnover of individual cells. Finally, the robust growth and temporary expansion of rod outer segments does not fit with a model of vascular insufficiency.

Photoreceptors respond to light in multiple ways over a variety of time scales. For example, teleost photoreceptors undergo a retinomotor reflex whereby onset of darkness triggers rod inner segments to contract and cone inner segments to elongate, with the reverse happening upon transition to light.[70] Importantly, retinomotor movements appear relatively late in development (after 20 dpf) and so cannot underlie the inner segment and positioning abnormalities in the *gdf6a* mutants, which appear as early as 4 dpf. Moreover, the layering of the mutant photoreceptors normalized before the onset of retinomotor movements (Fig. S4). Finally, the inner segments of both rods and cones are shorter in the mutants, which contrasts with the opposite movements of the two cell types in response to light.

Nevertheless, recent evidence suggests that light exposure does affect the morphologic development of the larval zebrafish photoreceptors.[39] Further, we found the disrupted layering of the photoreceptors in 5 dpf *gdf6a* mutants, with rod outer segments ectopically positioned basal to cone outer segments, resembles the older dark-adapted retinas.[70] The control and mutant fish were treated identically, with light adaptation before fixation, and exposure to a 14 hour:10 hour light:dark cycle after 5 dpf. One possibility is that improper focusing of light onto the mutant retinas leads to the observed photoreceptor changes. Indeed, previous work showed changes to lens development in the *gdf6a* mutants[20] and we observed here an overgrowth of the RPE, albeit subsequent to the onset of photoreceptor changes. However, the lens is not opaque in the mutants, and in some cases is even abnormally large relative to eye size (Fig. 2B), and light can still enter the larval mutant eye. It would be surprising if a partial light blockage would have such a profound effect on early morphologic development, but perhaps there is a feedback mechanism to modify the photoreceptors, similar to the myopia-inducing growth of the entire eye in response to form deprivation.[71] Regardless of the particular external cause of the phenotype, there must still be an underlying genetic response of the cells that is misdirecting photoreceptor maturation.

The RNA-Seq experiment revealed expected changes in cone- and rod-specific genes, most of which code for outer segment proteins and therefore matched the enlarged rod/reduced cone outer segment phenotype. Although most of the changes are likely a consequence of outer segment size, previous work established that manipulation of rhodopsin expression levels directly determines rod outer segment size.[18] But altered rhodopsin and cone opsin expression may be part of the mechanism underlying the mutant phenotype, it does not explain the changes to the inner segments or the abnormal layering of the photoreceptors in mutant larval fish.

Despite changes to the inner segment morphology of both rods and cones, we found little evidence for the misregulation of genes coding for inner segment proteins, such as those associated with the mitochondria, the cytoskeleton, or cell polarity. In addition, the mitochondrial ultrastructure was unchanged, and neither cell polarity nor cell–cell adhesions were disrupted in the outer nuclear layer. However, the structure of the outer segment is dependent on inner segment support, both through ongoing supply of energy and cellular components and via polarity proteins such as Crumbs, and we cannot discount the possibility that changes to the outer segments arise in the inner segment.

Crumbs transmembrane proteins are necessary for defining the apical compartment of photoreceptors, which includes the outer segment and most of the inner segment, as well as mediating interactions between photoreceptors.[44,48] Previous work revealed connections between Crumbs and photoreceptor morphology in zebrafish: overexpression of truncated Crb2a proteins (intracellular domain alone, extracellular domain with or without transmembrane domain) led to expanded rod outer segments, overexpression of full-length Crb2a resulted in expanded myoid regions,[47] and knockdown of Crb2b led to smaller red/green cones.[49] Further, Crumbs is negatively regulated by Mosaic eyes (Moe), and rods lacking Moe have expanded outer segments.[72]

The ability of Crumbs to control cell morphology is primarily through modification of the actin cytoskeleton, via either interactions with actin-binding proteins or regulation of small Rho GTPases.[73] Although the expression of *crumbs* genes is unchanged in the *gdf6a* mutants, both the Crb2a protein domain and the inner segment actin fibers were significantly shortened in apical-basal extent. It is unclear, however, whether either finding may have a role in creating the observed outer segment phenotypes in the mutant fish, or are simply a secondary consequence of the reduced inner segments.

Our data highlight gene expression changes associated with a unique photoreceptor phenotype. Although we do not yet have a clear of understanding of what is disrupting photoreceptor growth, we now have a list of genes associated with decreased growth of cone inner and outer segments, dysmorphic rod inner segments and robust growth of rod outer segments. Homologues of two downregulated genes, *KCNV2* and *TMEM237*, are of interest because of their associations with retinal dystrophies.[52,53,63] Further, the endogenous functions of the proteins and how their disruption leads to particular ocular disease phenotypes remain unclear and would be of interest in future studies.

Although the photoreceptors in *gdf6a* mutants have abnormal morphologies, the cells make properly organized outer segments. Further, the stunted cone outer segment phenotype is maintained over time while the rod outer

segment overgrowth recovers; both are phenotypes that diverge significantly from those caused by mutations in core outer segment genes, which typically lead to progressive degeneration.[3] Therefore, the *gdf6a* mutants offer a unique opportunity to examine nonessential factors that differentially regulate rod and cone outer segment growth.

References

1. Kumaran N, Moore AT, Weleber RG, Michaelides M. Leber congenital amaurosis/early-onset severe retinal dystrophy: clinical features, molecular genetics and therapeutic interventions. *Br J Ophthalmol*. 2017;101:1147–1154. doi: 10.1136/bjophthalmol-2016-309975

2. Goldberg AFX, Moritz OL, Williams DS. Molecular basis for photoreceptor outer segment architecture. *Prog Retin Eye Res*. 2016;55:52–81. doi: 10.1016/j.preteyeres.2016.05.003

3. Wensel TG, Zhang Z, Anastassov IA, et al. Structural and molecular bases of rod photoreceptor morphogenesis and disease. *Prog Retin Eye Res*. 2016;55:32–51. doi: 10.1016/j.preteyeres.2016.06.002

4. Baker SA, Kerov V. Photoreceptor inner and outer segments. *Curr Top Membr*. 2013;72:231–265. doi: 10.1016/B978-0-12-417027-8.00007-6

5. Insinna C, Besharse JC. Intraflagellar transport and the sensory outer segment of vertebrate photoreceptors. *Dev Dyn Off Publ Am Assoc Anat*. 2008;237:1982–1992. doi: 10.1002/dvdy.21554

6. Lamb TD. Why rods and cones? *Eye Lond Engl*. 2016;30:179–185. doi: 10.1038/eye.2015.236

7. Burgoyne T, Meschede IP, Burden JJ, Bailly M, Seabra MC, Futter CE. Rod disc renewal occurs by evagination of the ciliary plasma membrane that makes cadherin-based contacts with the inner segment. *Proc Natl Acad Sci USA*. 2015;112:15922–15927. doi: 10.1073/pnas.1509285113

8. Ding J-D, Salinas RY, Arshavsky VY. Discs of mammalian rod photoreceptors form through the membrane evagination mechanism. *J Cell Biol*. 2015;211:495–502. doi: 10.1083/jcb.201508093

9. Volland S, Hughes LC, Kong C, et al. Three-dimensional organization of nascent rod outer segment disk membranes. *Proc Natl Acad Sci USA*. 2015;112:14870–14875. doi: 10.1073/pnas.1516309112

10. Bilotta J, Saszik S. The zebrafish as a model visual system. *Int J Dev Neurosci Off J Int Soc Dev Neurosci*. 2001;19:621–629.

11. Malicki J, Pooranachandran N, Nikolaev A, Fang X, Avanesov A. Analysis of the retina in the zebrafish model. *Methods Cell Biol*. 2016;134:257–334. doi: 10.1016/bs.mcb.2016.04.017

12. Bujakowska KM, Liu Q, Pierce EA. Photoreceptor cilia and retinal ciliopathies. *Cold Spring Harb Perspect Biol*. 2017;9. doi: 10.1101/cshperspect.a028274

13. Estrada-Cuzcano A, Roepman R, Cremers FPM, den Hollander AI, Mans DA. Non-syndromic retinal ciliopathies: translating gene discovery into therapy. *Hum Mol Genet*. 2012;21:R111–124. doi: 10.1093/hmg/dds298

14. Taub DG, Liu Q. The role of intraflagellar transport in the photoreceptor sensory cilium. *Adv Exp Med Biol*. 2016;854:627–633. doi: 10.1007/978-3-319-17121-0_83

15. Salinas RY, Pearring JN, Ding J-D, Spencer WJ, Hao Y, Arshavsky VY. Photoreceptor discs form through peripherin-dependent suppression of ciliary ectosome release. *J Cell Biol*. 2017;216:1489–1499. doi: 10.1083/jcb.201608081

16. Hollingsworth TJ, Gross AK. Defective trafficking of rhodopsin and its role in retinal degenerations. *Int Rev Cell Mol Biol*. 2012;293:1–44. doi: 10.1016/B978-0-12-394304-0.00006-3

17. Nemet I, Ropelewski P, Imanishi Y. Rhodopsin trafficking and mistrafficking: signals, molecular components, and mechanisms. *Prog Mol Biol Transl Sci*. 2015;132:39–71. doi: 10.1016/bs.pmbts.2015.02.007

18. Price BA, Sandoval IM, Chan F, et al. Rhodopsin gene expression determines rod outer segment size and rod cell resistance to a dominant-negative neurodegeneration mutant. *PLoS One*. 2012;7:e49889. doi: 10.1371/journal.pone.0049889

19. Amram B, Cohen-Tayar Y, David A, Ashery-Padan R. The retinal pigmented epithelium - from basic developmental biology research to translational approaches. *Int J Dev Biol*. 2017;61:225–234. doi: 10.1387/ijdb.160393ra

20. French CR, Erickson T, French DV, Pilgrim DB, Waskiewicz AJ. Gdf6a is required for the initiation of dorsal-ventral retinal patterning and lens development. *Dev Biol*. 2009;333:37–47. doi: 10.1016/j.ydbio.2009.06.018

21. French CR, Stach TR, March LD, Lehmann OJ, Waskiewicz AJ. Apoptotic and proliferative defects characterize ocular development in a microphthalmic BMP model. *Invest Ophthalmol Vis Sci*. 2013;54:4636–4647. doi: 10.1167/iovs.13-11674

22. Gosse NJ, Baier H. An essential role for Radar (Gdf6a) in inducing dorsal fate in the zebrafish retina. *Proc Natl Acad Sci USA*. 2009;106:2236–2241. doi: 10.1073/pnas.0803202106

23. Hocking JC, Famulski JK, Yoon KH, et al. Morphogenetic defects underlie superior coloboma, a newly identified closure disorder of the dorsal eye. *PLoS Genet*. 2018;14:e1007246. doi: 10.1371/journal.pgen.1007246

24. den Hollander AI, Biyanwila J, Kovach P, et al. Genetic defects of GDF6 in the zebrafish out of sight mutant and in human eye developmental anomalies. *BMC Genet*. 2010;11:102. doi: 10.1186/1471-2156-11-102

25. Kruse-Bend R, Rosenthal J, Quist TS, et al. Extraocular ectoderm triggers dorsal retinal fate during optic vesicle evagination in zebrafish. *Dev Biol*. 2012;371:57–65. doi: 10.1016/j.ydbio.2012.08.004

26. Valdivia LE, Lamb DB, Horner W, et al. Antagonism between Gdf6a and retinoic acid pathways controls timing of retinal neurogenesis and growth of the eye in zebrafish. *Dev Camb Engl*. 2016;143:1087–1098. doi: 10.1242/dev.130922

27. Asai-Coakwell M, French CR, Berry KM, et al. GDF6, a novel locus for a spectrum of ocular developmental anomalies. *Am J Hum Genet*. 2007;80:306–315. doi: 10.1086/511280

28. Asai-Coakwell M, March L, Dai XH, et al. Contribution of growth differentiation factor 6-dependent cell survival to early-onset retinal dystrophies. *Hum Mol Genet*. 2013;22:1432–1442. doi: 10.1093/hmg/dds560

29. Hamaoka T, Takechi M, Chinen A, Nishiwaki Y, Kawamura S. Visualization of rod photoreceptor development using GFP-transgenic zebrafish. *Genes N Y N 2000*. 2002;34:215–220. doi: 10.1002/gene.10155

30. Takechi M, Hamaoka T, Kawamura S. Fluorescence visualization of ultraviolet-sensitive cone photoreceptor development in living zebrafish. *FEBS Lett*. 2003;553:90–94.

31. Salbreux G, Barthel LK, Raymond PA, Lubensky DK. Coupling mechanical deformations and planar cell polarity to create regular patterns in the zebrafish retina. *PLoS Comput Biol*. 2012;8:e1002618. doi: 10.1371/journal.pcbi.1002618

32. Raymond PA, Colvin SM, Jabeen Z, et al. Patterning the cone mosaic array in zebrafish retina requires specification of ultraviolet-sensitive cones. *PLoS ONE*. 2014; 34:e85325. doi: 10.1371/journal.pone.0085325

33. Doganli C, Bukata L, Lykke-Hartmann K. Whole-mount immunohistochemistry for anti-F59 in zebrafish embryos (1-5 days post fertilization (dpf)). *Methods Mol Biol Clifton NJ*. 2016;1377:365–369. doi: 10.1007/978-1-4939-3179-8_32

34. Bray NL, Pimentel H, Melsted P, Pachter L. Near-optimal probabilistic RNA-seq quantification. *Nat Biotechnol*. 2016;34:525–527. doi: 10.1038/nbt.3519

35. Pimentel H, Bray NL, Puente S, Melsted P, Pachter L. Differential analysis of RNA-seq incorporating quantification uncertainty. *Nat Methods*. 2017;14:687–690. doi: 10.1038/nmeth.4324

36. Bustin SA, Benes V, Garson JA, et al. The MIQE guidelines: minimum information for publication of quantitative real-time PCR experiments. *Clin Chem*. 2009;55:611–622. doi: 10.1373/clinchem.2008.112797

37. Ginzinger DG. Gene quantification using real-time quantitative PCR: an emerging technology hits the mainstream. *Exp Hematol*. 2002;30:503–512. doi: 10.1016/s0301-472x(02)00806-8

38. Gaetano J. Welch's t-test for comparing two independent groups: an Excel calculator (1.0.1) [Microsoft Excel workbook]. Retrieved from: https://www.researchgate.net/publication/332217175_. doi: 10.13140/RG.2.2.14550.91209/2

39. Crespo C, Knust E. Characterisation of maturation of photoreceptor cell subtypes during zebrafish retinal development. *Biol Open*. 2018;7. doi: 10.1242/bio.036632

40. Stuck MW, Conley SM, Naash MI. PRPH2/RDS and ROM-1: historical context, current views and future considerations. *Prog Retin Eye Res*. 2016;52:47–63. doi: 10.1016/j.preteyeres.2015.12.002

41. DuVal MG, Allison WT. Photoreceptor progenitors depend upon coordination of gdf6a, thrβ, and tbx2b to generate precise populations of cone photoreceptor subtypes. *Invest Ophthalmol Vis Sci*. 2018;59:6089–6101. doi: 10.1167/iovs.18-24461

42. Duval MG, Oel AP, Allison WT. gdf6a is required for cone photoreceptor subtype differentiation and for the actions of tbx2b in determining rod versus cone photoreceptor fate. *PloS One*. 2014;9:e92991. doi: 10.1371/journal.pone.0092991

43. Calvo SE, Clauser KR, Mootha VK. MitoCarta2.0: an updated inventory of mammalian mitochondrial proteins. *Nucleic Acids Res*. 2016;44(D1):D1251–1257. doi: 10.1093/nar/gkv1003

44. Pocha SM, Knust E. Complexities of Crumbs function and regulation in tissue morphogenesis. *Curr Biol CB*. 2013;23:R289–293. doi: 10.1016/j.cub.2013.03.001

45. Alves CH, Pellissier LP, Vos RM, et al. Targeted ablation of Crb2 in photoreceptor cells induces retinitis pigmentosa. *Hum Mol Genet*. 2014;23:3384–3401. doi: 10.1093/hmg/ddu048

46. Ehrenberg M, Pierce EA, Cox GF, Fulton AB. CRB1: one gene, many phenotypes. *Semin Ophthalmol*. 2013;28(5-6):397–405. doi: 10.3109/08820538.2013.825277

47. Hsu Y-C, Jensen AM. Multiple domains in the Crumbs homolog 2a (Crb2a) protein are required for regulating rod photoreceptor size. *BMC Cell Biol*. 2010;11:60. doi: 10.1186/1471-2121-11-60

48. Zou J, Wang X, Wei X. Crb apical polarity proteins maintain zebrafish retinal cone mosaics via intercellular binding of their extracellular domains. *Dev Cell*. 2012;22:1261–1274. doi: 10.1016/j.devcel.2012.03.007

49. Omori Y, Malicki J. oko meduzy and related crumbs genes are determinants of apical cell features in the vertebrate embryo. *Curr Biol CB*. 2006;16:945–957. doi: 10.1016/j.cub.2006.03.058

50. Nagle BW, Okamoto C, Taggart B, Burnside B. The teleost cone cytoskeleton. Localization of actin, microtubules, and intermediate filaments. *Invest Ophthalmol Vis Sci*. 1986;27:689–701.

51. Beech DJ, Barnes S. Characterization of a voltage-gated K+ channel that accelerates the rod response to dim light. *Neuron*. 1989;3:573–581.

52. Wissinger B, Dangel S, Jägle H, et al. Cone dystrophy with supernormal rod response is strictly associated with mutations in KCNV2. *Invest Ophthalmol Vis Sci*. 2008;49:751–757. doi: 10.1167/iovs.07-0471

53. Wu H, Cowing JA, Michaelides M, et al. Mutations in the gene KCNV2 encoding a voltage-gated potassium channel subunit cause "cone dystrophy with supernormal rod electroretinogram" in humans. *Am J Hum Genet*. 2006;79:574–579. doi: 10.1086/507568

54. Michaelides M, Holder GE, Webster AR, et al. A detailed phenotypic study of "cone dystrophy with supernormal rod ERG". *Br J Ophthalmol*. 2005;89:332–339. doi: 10.1136/bjo.2004.050567

55. Sun C, Galicia C, Stenkamp DL. Transcripts within rod photoreceptors of the Zebrafish retina. *BMC Genomics*. 2018;19:127. doi: 10.1186/s12864-018-4499-y

56. Omri S, Omri B, Savoldelli M, et al. The outer limiting membrane (OLM) revisited: clinical implications. *Clin Ophthalmol Auckl NZ*. 2010;4:183–195.

57. Williams DS, Arikawa K, Paallysaho T. Cytoskeletal components of the adherens junctions between the photoreceptors and the supportive Müller cells. *J Comp Neurol*. 1990;295:155–164. doi: 10.1002/cne.902950113

58. Fleisch VC, Neuhauss SCF. Parallel visual cycles in the zebrafish retina. *Prog Retin Eye Res*. 2010;29:476–486. doi: 10.1016/j.preteyeres.2010.05.001

59. Wang J-S, Kefalov VJ. The cone-specific visual cycle. *Prog Retin Eye Res*. 2011;30:115–128. doi: 10.1016/j.preteyeres.2010.11.001

60. Fleisch VC, Schonthaler HB, von Lintig J, Neuhauss SCF. Subfunctionalization of a retinoid-binding protein provides evidence for two parallel visual cycles in the cone-dominant zebrafish retina. *J Neurosci Off J Soc Neurosci*. 2008;28:8208–8216. doi: 10.1523/JNEUROSCI.2367-08.2008

61. Campbell LJ, Jensen AM. Phosphodiesterase inhibitors sildenafil and vardenafil reduce zebrafish rod photoreceptor outer segment shedding. *Invest Ophthalmol Vis Sci*. 2017;58:5604–5615. doi: 10.1167/iovs.17-21958

62. Gross JM, Perkins BD, Amsterdam A, et al. Identification of zebrafish insertional mutants with defects in visual system

development and function. *Genetics*. 2005;170:245–261. doi: 10.1534/genetics.104.039727

63. Huang L, Szymanska K, Jensen VL, et al. TMEM237 is mutated in individuals with a Joubert syndrome related disorder and expands the role of the TMEM family at the ciliary transition zone. *Am J Hum Genet*. 2011;89:713–730. doi: 10.1016/j.ajhg.2011.11.005

64. Zuniga FI, Craft CM. Deciphering the structure and function of Als2cr4 in the mouse retina. *Invest Ophthalmol Vis Sci*. 2010;51:4407–4415. doi: 10.1167/iovs.10-5251

65. Bilotta J, Saszik S, Sutherland SE. Rod contributions to the electroretinogram of the dark-adapted developing zebrafish. *Dev Dyn Off Publ Am Assoc Anat*. 2001;222:564–570. doi: 10.1002/dvdy.1188

66. Vecino E, Rodriguez FD, Ruzafa N, Pereiro X, Sharma SC. Glia-neuron interactions in the mammalian retina. *Prog Retin Eye Res*. 2016;51:1–40. doi: 10.1016/j.preteyeres.2015.06.003

67. Country MW. Retinal metabolism: a comparative look at energetics in the retina. *Brain Res*. 2017;1672:50–57. doi: 10.1016/j.brainres.2017.07.025

68. Kurihara T, Westenskow PD, Gantner ML, et al. Hypoxia-induced metabolic stress in retinal pigment epithelial cells is sufficient to induce photoreceptor degeneration. *eLife*. 2016;5. doi: 10.7554/eLife.14319

69. Stefánsson E, Geirsdóttir A, Sigurdsson H. Metabolic physiology in age related macular degeneration. *Prog Retin Eye Res*. 2011;30:72–80. doi: 10.1016/j.preteyeres.2010.09.003

70. Hodel C, Neuhauss SCF, Biehlmaier O. Time course and development of light adaptation processes in the outer zebrafish retina. *Anat Rec A Discov Mol Cell Evol Biol*. 2006;288:653–662. doi: 10.1002/ar.a.20329

71. Schaeffel F, Feldkaemper M. Animal models in myopia research. *Clin Exp Optom*. 2015;98:507–517. doi: 10.1111/cxo.12312

72. Hsu Y-C, Willoughby JJ, Christensen AK, Jensen AM. Mosaic eyes is a novel component of the Crumbs complex and negatively regulates photoreceptor apical size. *Dev Camb Engl*. 2006;133:4849–4859. doi: 10.1242/dev.02685

73. Bazellières E, Aksenova V, Barthélémy-Requin M, Massey-Harroche D, Le Bivic A. Role of the Crumbs proteins in ciliogenesis, cell migration and actin organization. *Semin Cell Dev Biol*. 2018;81:13–20. doi: 10.1016/j.semcdb.2017.10.018